Applied Physics B (2018) 124:145
https://doi.org/10.1007/s00340-018-7015-9

Applied Physics B
Lasers and Optics

Axial coherent emissions controlled by an internal coupling field in an open four-level potassium system

N. Merlemis[1] · G. Papademetriou[2] · D. Pentaris[2] · T. Efthimiopoulos[2] · V. Vaičaitis[3]

Received: 29 August 2017 / Accepted: 20 June 2018 / Published online: 23 June 2018

Abstract
We present a theoretical model interpreting the experimental results observed under strong two-photon ns laser excitation of the $|6S_{1/2}\rangle$ potassium atomic state, where emissions near the $|6S_{1/2}\rangle \leftrightarrow |4P_{3/2}\rangle$ and $|4P_{3/2}\rangle \leftrightarrow |4S_{1/2}\rangle$ transitions were experimentally observed. It is shown that the $|6S_{1/2}\rangle \leftrightarrow |4P_{3/2}\rangle$ emission initially grows nonlinearly with pump intensity, while subsequently saturates and enhances the generation of radiation near the $|4P_{3/2}\rangle \leftrightarrow |4S_{1/2}\rangle$ transition. It is found that a coherent manipulation of an open four-level system is possible by an internally generated, saturated coupling field, despite the energy decay to the continuum. The efficiency of the proposed coherent control method is managed by adjusting the pump intensity and potassium density. Finally, a general control scheme is discussed in which an external pump and an internal coupling field determine the system's response in a cascade scheme.

1 Introduction

Four-wave mixing (FWM) processes were extensively studied in order to generate coherent radiation in various spectral regions [1–9]. A laser field is usually tuned near a two-photon transition in order to enhance the third-order susceptibility and a second laser couples the two-photon resonant state to a discrete atomic state or a broad auto-ionizing one. This method was applied to further increase the nonlinear susceptibility $\chi^{(3)}$, therefore obtaining an extended tuning range for the generation of radiation and also avoiding the large on-resonance absorption [1, 2]. In such FWM processes the two laser fields are externally provided to the atomic medium. However, there is an alternative mixing process which involves only a single external pump connecting the ground level to a two-photon resonant state. In this case, the atomic response consists of a parametric four-wave mixing (PFWM) process that includes the simultaneous generation of two coherent fields, which are phase matched near an intermediate state. Axial phase-matching, either by adding a rare gas or by self-adjustment of the emission wavelength, and conical phase-matching, by self-adjustment of the emission angle, have already been observed for ns [3–6], ps [7] and fs [8, 9] pulses.

In PFWM there is no significant population transfer from the ground state and there is no substantial temporal delay between the emitted fields and the driving laser pulse. A method to enhance the efficiency of the FWM process was proposed in [10]. According to this method, a strong coupling field is applied between the two-photon resonant, metastable, intermediate level and the upper state involved in the mixing. This enhances the nonlinear susceptibility of the medium and thus the yield of the generated radiation, while, under certain conditions, it also induces a window in the absorption from the ground state to the upper one. The reduced absorption and the enhancement of nonlinear wave mixing processes due to electromagnetically induced transparency (EIT) have been experimentally demonstrated [11–16]. Most experiments related to coherent mixing and EIT use two laser fields to couple the atomic system states in a *V*, *Λ* or cascade configuration.

In this work, emissions in a cascade scheme through $|6S_{1/2}\rangle \leftrightarrow |4P_{3/2}\rangle \leftrightarrow |4S_{1/2}\rangle$ states of the potassium atom

✉ G. Papademetriou
gpapadem@gmail.com

[1] Department of Surveying & Geoinformatics Engineering, University of West Attica, Athens 12243, Greece

[2] Laser, Nonlinear and Quantum Optics Labs, Physics Department, University of Patras, Patras 26500, Greece

[3] Vilnius University Laser Research Center, Sauletekio 10, Vilnius 10223, Lithuania

are internally generated when a ns or fs excitation pump couples the $|6S_{1/2}\rangle$ state to the ground $|4S_{1/2}\rangle$ one. Figure 1 depicts the energy-level diagram appropriate for this study. It was shown [17–22] that a two-photon excitation tuned on or above the $|6S_{1/2}\rangle$ state can produce amplified spontaneous emission (ASE), as a result of cascading to lower empty levels such as the $|4P\rangle$ levels, and stimulated hyper Raman scattering (SHRS) in the $|6S_{1/2}\rangle \leftrightarrow |5P_{3/2}\rangle$ and $|6S_{1/2}\rangle \leftrightarrow |5P_{1/2}\rangle$ transitions. Parametrically generated four-wave mixing (PFWM) radiation, which involves the incoming photons (pump) and the internally generated ones along the direction of the incoming excitation beam, was also observed [23]. Moreover, a competition due to quantum interference effects between ASE or SHRS and the PFWM processes leads to the suppression of ASE and SHRS [24–27]. More recent experimental and theoretical works [28–35] examined the laser-atom interaction under a single laser excitation and the role of destructive quantum interference (QI) in more detail. It was found that the destructive QI can modify the nonlinearity of the $|6S_{1/2}\rangle \leftrightarrow |5P_{3/2}\rangle \leftrightarrow |4S_{1/2}\rangle$atomic path in potassium [3, 4, 33–37] when the excitation laser intensity is sufficiently strong for a certain atomic density. The latter was seen as a method to coherently control PFWM emissions [38–40].

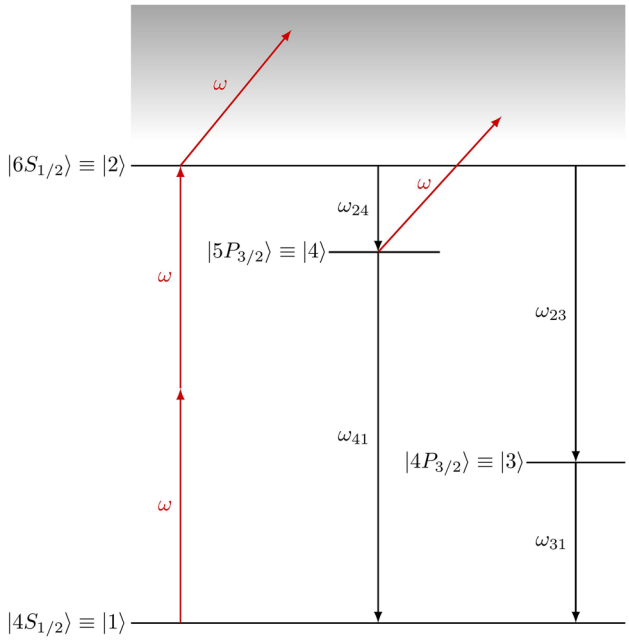

Fig. 1 A schematic energy-level diagram of potassium atom is shown. The emissions near $|2\rangle \leftrightarrow |4\rangle$, $|4\rangle \leftrightarrow |1\rangle$, $|2\rangle \leftrightarrow |3\rangle$ and $|3\rangle \leftrightarrow |1\rangle$ transitions, are internally generated in the medium. The two-photon resonant, three-photon ionization, (3ω), from the $|2\rangle$ state as well as the single-photon transition (ω) to continuum from the $|4\rangle$ state are depicted. The frequencies of the internally emitted fields are denoted as ω_{24}, ω_{41}, ω_{23} and ω_{31}, respectively

Taking into account past results in the field [24–41], we investigate the case where partially coherent emissions such as ASE or SHRS and FWM can be effectively controlled under conditions of strong laser fields (focused beams). We present experimental results and a theoretical model which indicate that a strong internally generated ASE near the $|6S_{1/2}\rangle \leftrightarrow |4P_{3/2}\rangle$ transition acts as a coupling field, enhancing ASE or FWM radiation from the $|4P_{3/2}\rangle$ state to the ground level. Elevated atomic density decreases the efficiency of the process. It is shown that when the ASE at the upper transition ($|6S_{1/2}\rangle \leftrightarrow |4P_{3/2}\rangle$) is saturated, the pumping energy is transferred to the lower transition $|4P_{3/2}\rangle \leftrightarrow |4S_{1/2}\rangle$with higher efficiency. The proposed method uses only a single external laser field and the experiments are performed at high pumping intensities, in contrast to other works [38–41] of our group. An open four-level system is applied in the theoretical description of the system, including the mechanism of ionization losses to the continuum [36, 37], with the parameters of the model simulating the experimental conditions. Finally, a general control scheme is proposed including an external pump and internal coupling fields in a cascade configuration that has been shown to enhance the nonlinear response in similar systems.

2 Experiment

In the experiment, the potassium atoms were confined inside a stainless-steel heat-pipe oven of ζ_L =17 cm active vapor length. The potassium vapor density could be varied between 10^{14} and 10^{16} cm^{-3}, while helium (He) or argon (Ar) were used as buffer gas to keep the potassium atoms away from the heat-pipe windows and also could be used for phase-matching if needed. A stainless-steel electrode along the pipe axis was used for recording the exact two-photon resonance from the ionization signal. An excimer–pumped dye laser having a bandwidth of 0.1 cm^{-1} and pulse duration of 25 ns was employed as the ns excitation source, for the two-photon $|4S_{1/2}\rangle \leftrightarrow |6S_{1/2}\rangle$ transition of potassium. The maximum energy available was 5 mJ per pulse. In the case of strong excitation (focused beam) the beam diameter was approximately 2 mm, before entering the lens ($F = 20$ cm). The calculated beam waist at the center of the pipe was $w_0 = 23$ μm, leading to a maximum laser intensity of $I_L = 94$ GW/cm^2.

In addition, a second fs pump laser with single pulse energy of about 125 μJ was used in a similar experimental

setup. An optical parametric generator, OPO ("Light conversion", Topas), pumped by a fs Ti:sapphire laser ("Coherent", Libra-USP-HE), delivered pulses having a full-width-half-maximum (FWHM) duration of 40 fs, a FWHM spectral bandwidth of 10 nm and a repetition rate of 1 kHz. The beam diameter was approximately 2–3 mm and it was focused by a 30 cm focal length lens, into the vapor cell center with an estimated intensity of $I_p = 20\ \mathrm{TW}/\mathrm{cm}^2$. A set of fiber, a digital spectrometer and a computer were used to record the emitted spectra, using appropriate interference and neutral density filters. The frequency–angular distributions of the conical emissions were recorded with an imaging spectrometer Andor SR-500i-D1 by placing its entrance slit in the focal plane of a focusing lens. Under such configuration the spectrometer disperses the light energy across the spectral range and produces a 2-dimensional image at the output imaging plane (the vertical coordinate is proportional to the light direction). Assuming the axial symmetry of the emissions and by placing a CCD camera in the output imaging plane of the spectrometer the frequency–angular distributions can be captured in a single shot.

3 Simplified theoretical model

The potassium atom is modeled as an open four-level system, since the transition to the continuum is taken into account, as shown in Fig. 1. An external laser pulse with FWHM $\tau_c = 25$ ns and waveform $\sec h^2\left(\left(\tau - \tau_c\right)/\tau_c\right)$ for $\tau < 0$ and $e^{-(\tau-\tau_c)^2/\tau_c^2}$ for $\tau > 0$, is used, in order to simulate the asymmetric Gaussian envelope of the ns excimer–dye pulse. The notation $|1\rangle$, $|2\rangle$, $|3\rangle$, $|4\rangle$ corresponds to the $\left|4S_{1/2}\right\rangle$, $\left|6S_{1/2}\right\rangle$, $\left|4P_{3/2}\right\rangle$ and $\left|5P_{3/2}\right\rangle$ states. The emitted fields are internally generated at frequencies ω_{24}, ω_{41}, ω_{23} and ω_{31}, which correspond to the $\left|6S_{1/2}\right\rangle \leftrightarrow \left|5P_{3/2}\right\rangle$, $\left|5P_{3/2}\right\rangle \leftrightarrow \left|4S_{1/2}\right\rangle$ transitions (path-1), and the $\left|6S_{1/2}\right\rangle \leftrightarrow \left|4P_{3/2}\right\rangle$, $\left|4P_{3/2}\right\rangle \leftrightarrow \left|4S_{1/2}\right\rangle$ ones (path-2) [33, 34].

We note that for a complete study of potassium atom the $\left|4P_{1/2}\right\rangle$ and $\left|5P_{1/2}\right\rangle$ states should be included as well. However, there are certain reasons (experimental data) which justify the chosen four-level configuration. Specifically, the emissions of the doublet $\left|5P_{3/2}\right\rangle \leftrightarrow \left|4S_{1/2}\right\rangle$ and $\left|5P_{1/2}\right\rangle \leftrightarrow \left|4S_{1/2}\right\rangle$ transitions are merged in a single peak when the pump laser is focused [3, 4], and the $\left|4P_{3/2}\right\rangle \leftrightarrow \left|4S_{1/2}\right\rangle$ transition has the strongest coupling to the ground state among the two $|4P\rangle$ states [3, 4]. In the interaction picture the atomic system Hamiltonian has the following form:

$$H_I^{(I)} = -\hbar\Big(\Omega_{12}^{(2)}|1\rangle\langle 2|e^{-i\Delta_{12}t} + \Omega_{14}|1\rangle\langle 4|e^{-i\Delta_{14}t} + \Omega_{13}|1\rangle\langle 3|e^{-i\Delta_{13}t} + \Omega_{32}|3\rangle\langle 2|e^{-i\Delta_{23}t} + \Omega_{42}|4\rangle\langle 2|e^{-i\Delta_{24}t} + \mathrm{h.c.}\Big),$$

where $\Omega_{12}^{(2)}$ is the two-photon Rabi frequency, and Ω_{42}, Ω_{14}, Ω_{32}, Ω_{13} are the single-photon Rabi frequencies, respectively. $\Delta_{ij} = \nu_{ij} - \omega_{ij}$ is the detuning of $|i\rangle \leftrightarrow |j\rangle$ transition, where ν_{ij} is the frequency of the electric field related to the transition $|i\rangle \leftrightarrow |j\rangle$ (with $\{i,j\} = \{1,4\}$ and $i \neq j$). From the von Neumann equation $\dot{\rho} = -i/\hbar\left[H_I^{(I)}, \rho\right]$ in the rotating wave approximation (RWA) a system of 16 density matrix equations is formed [33], where the decaying rates γ_{ij} and the elastic collision dephasing ones γ_{col} are added phenomenologically.

In order to include the transition to the continuum through the two-photon resonant, three-photon ionization mechanism, the model has to be transformed. At first, the summation of the population derivatives is non-zero, in contrast to a close system. The formula $\sum_{ii=1}^{4}\left(\mathrm{d}\sigma_{ii}(\zeta,\tau)/\mathrm{d}\tau\right) = -\Gamma_{ion} I_{max} F(\tau)\sigma_{22}$ holds in the modified set of equations. I_{max} is the laser peak intensity and Γ_{ion} is the ionization width. More information about the ionization rate in an open atomic system can be found in references [36–40]. In addition, the term $-\Gamma_{ion} I_{max} F(\tau)\sigma_{mn}/2$ is included in the set of equations (7), (9) and (10) of reference [33]. It is obvious that all transitions connected with state $|2\rangle$ are affected by the transition to the continuum (quantified by the factor Γ_{ion}) due to the two-photon resonant, three-photon ionization process. Furthermore, an alternative term $-\Gamma'_{ion} I_{max} F(\tau)\sigma_{44}$ holds in the modified set of equations [33] if we assume system loses from state $|4\rangle$ to continuum. Subsequently, a new additional term $-\Gamma'_{ion} I_{max} F(\tau)\sigma_{mn}/2$ has to be introduced in the set of equations (6), (8) and (10) [33], related to the off-diagonal matrix elements σ_{mn}. The ionization width values Γ_{ion}, Γ'_{ion} are taken from reference [36, 37] in order to simulate the experimental conditions.

The Maxwell equations, with respect to the Rabi frequencies, in the slowly varying envelope approximation (SVEA), for the axially forward propagating waves, can be written in a general form: $\partial/\partial\zeta\left(\Omega_{mn}(\zeta,\tau)\right) = i\left(k_{mn}/4\varepsilon_0\hbar\right)\mu_{nm}p_{mn}(\zeta,\tau)$, with $\{m,n\} = \{2,4\}$. $p_{mn}(\zeta,\tau) = N\mathrm{Tr}(\mu\rho)$ is the quantum mechanical polarization, k_{mn} is the wave-number of each transition, ε_0 is the permittivity of free space, N is the atomic density and μ_{nm} is the matrix element of the electric dipole operator. The full system of coupled differential equations is solved numerically in order to define the unknown amplitudes Ω_{ij} of the Rabi frequencies and the density matrix elements σ_{ij}.

Finally, the boundary conditions of the numerical solution are: (a) the atoms lay in the ground state for each ζ at $\tau = 0$ and (b) the Rabi frequencies at $\zeta = 0$ are given by the quantum noise, with typical value $\Omega_{mn}(\zeta, \tau) \propto \varepsilon_{mn}(\zeta, \tau) = 10^{-4}$ V/cm [33, 34].

3.1 Approximations of the model

Several approximations have been applied to our simplified model, in order to take into account the experimental observations under both ns and fs excitation schemes. The propagation length in the model was chosen to include the vicinity of the focal region which, considering the Rayleigh length $z_R = (\pi/\lambda)w_0^2$ of the asymmetric Gaussian focused beam, equals to $\zeta_{max} = 2z_R$ or $\zeta_{max} = 0.46$ cm. In our model an asymmetric Gaussian pump (a secant square rising part and a Gaussian trailing one) excites the system. It should be mentioned that the excitation field is spatially more extended than the active atomic medium length ζ_{max} and no modification of the pump amplitude is necessary. In length units, the excitation field is equal to 750 cm and propagation effects of the pump are not taken into account.

The maximum laser peak intensity used in the model is set to be $I_{max} = 100$ MW/cm^2, which is three orders of magnitude less than the experimental one in the ns excitation case. This choice is justified by the fact that the experimental laser bandwidth of 0.1 cm^{-1} is much broader than the broadening of the excited $|2\rangle$ state (0.017 cm^{-1}) [34]. The latter means that there is a large overestimation of the laser energy provided to the atomic system in the case of the numerical calculations. The comparison of the numerical results with the experimental ones, as are presented below, indicates that the theoretical pump intensity should be lower by a factor of ~ 5000 in order to adequately simulate the experiment.

In addition, our model takes into account only the axially forward propagating fields, while, in the experiments, both forward and weak backward radiations were observed along with axial and conical features of the emissions, when the excitation laser was tuned on the two-photon resonance. Finally, the maximum atomic density used in the calculations has a value of $N_{max} = 3.5 \times 10^{15}$ cm^{-3}, similar to the experimental one.

It is important to note that in this work we focus on the interpretation of the experimental results taken under the ns excitation pumping scheme. However, experimental observations under a fs pump are also taken into consideration in the following discussion. Figure 2 shows the emission spectra of potassium atomic states $\left|4P_{3/2,1/2}\right\rangle$ and $\left|5P_{3/2,1/2}\right\rangle$, when the $\left|6S_{1/2}\right\rangle$ state is excited by a 40 fs laser of 10 nm bandwidth and 125 μJ pulse energy. A spectrometer which can record axial and off-axial emission was used. The presence of a threshold is clearly shown in Fig. 2a, where the intensity of the $\left|4P_{3/2,1/2}\right\rangle \leftrightarrow \left|4S_{1/2}\right\rangle$ emission is presented as a function of the excitation laser energy. The complex spatial profile of the emissions from the $|4P\rangle$ and $|5P\rangle$ states are evident in Fig. 2b–d, where it is clearly shown that radiation is emitted at large angles (angle phase-matched FWM) in the case of fs excitation. Therefore, our simplified model, which takes into account only axial propagation, fits better to the experimental results of the ns excitation scheme where axial emissions are dominant [3, 4].

As a result, the experimental data of Fig. 2 for the fs excitation are included in this work so that a comparison with the ns excitation is possible and also to indicate the approximations applied in our theoretical model. A complete analysis and discussion of the experimental results and the theoretical study of the fs excitation case will be presented in a forthcoming publication of our group.

4 Results and discussion

In the following, we present results for the $|4\rangle \leftrightarrow |1\rangle$ emission of path-1 (Sect. 4.1). The population distribution of the system is also shown. Subsequently, in Sect. 4.2, the emissions near $|2\rangle \leftrightarrow |3\rangle$ and $|3\rangle \leftrightarrow |1\rangle$ transitions of path-2 are presented in comparison to path-1.

Finally, we discuss in detail the response of path-2 for various values of laser intensity, as well as the atomic density effect for the maximum laser intensity used (Sect. 4.3), in an attempt to control the system's response. All the results were taken when the laser was tuned on the two-photon resonance.

4.1 Path-1

Figure 3a presents the normalized energy plot of the $|4\rangle \leftrightarrow |1\rangle$ emission for several pump intensities, a potassium–buffer gas collisions rate of $\gamma_{col} = 0.017$ cm^{-1} and for an atomic density of$N_{max} = 1.5 \times 10^{15}$ cm^{-3}, as were calculated by the model. The energy ε_{ij} of the emissions was estimated by the corresponding integrals of their temporal profiles. It is clear that the radiation at ω_{41} rises sharply for low pump intensities (nonlinear region), but saturates for pump intensities greater than $10^{-1} I_{max}$.

Similar response was observed in previous works [33, 34, 38–40] and it was explained by a similar model but without the use of the ionization path (closed system). Thus it is evident that path-1 is not affected much by the transition of the system to the continuum. We expected that ionization mainly affects the emissions which depend on the population redistribution, such as ASE or SHRS, rather than the coherent processes (PFWM) that lead to the emission at ω_{41} [33]. In Fig. 4, we show the population distribution for two

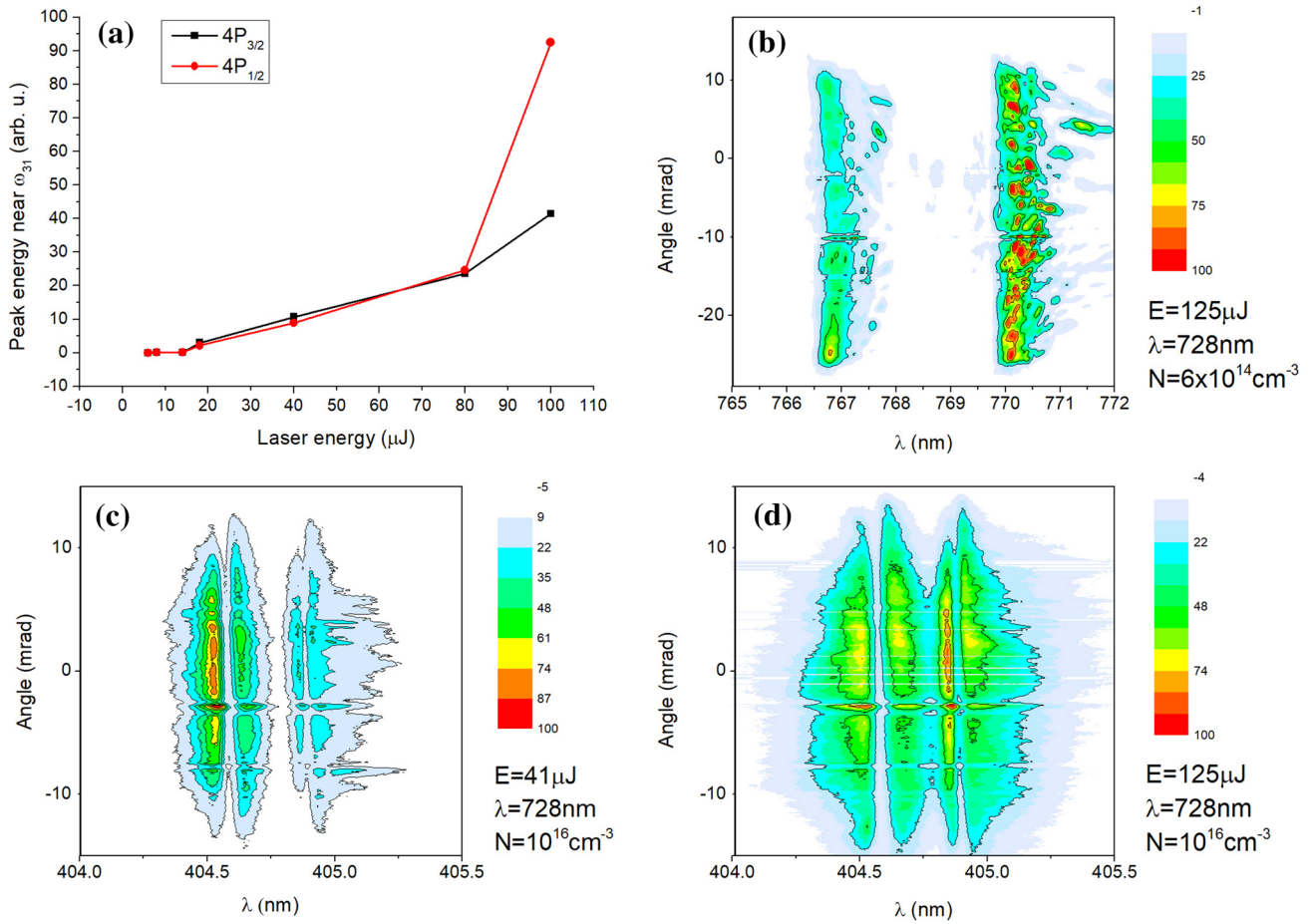

Fig. 2 **a** The $|4P\rangle - |4S\rangle$ emission intensity as a function of the pump laser energy. The potassium atoms are excited by a laser field of 40 fs temporal width and 10 nm spectral width tuned on two-photon resonance (728 nm laser wavelength). **b** The $|4P\rangle - |4S\rangle$ emission spectra at 6×10^{14} cm^{-3}density and for 125 μJ pump energy. **c, d** The $|5P\rangle - |4S\rangle$ emission spectra at 10^{16} cm^{-3} density for 41 and 125 μJ pump energy, respectively

different excitation intensities and for the density$N_{\max}$. In Fig. 4a, we observe the pronounced population redistribution between the involved states near the peak of the pump pulse ($\tau \approx 0$ ns). However, for high intensities (Fig. 4b), the populations' oscillation is considerably reduced in contrast to the calculations of a closed system [29, 33]. For the high pump intensity of Fig. 4c, the populations of the $|1\rangle$, $|2\rangle$ and $|3\rangle$ states decrease to a zero value near the pump maximum ($\tau \approx 0$). Population of the $|4\rangle$ state repopulates only the $|1\rangle$ state after the pump maximum, as expected, and there is no significant involvement of the $|2\rangle$ and $|3\rangle$ states in the system population anymore.

The large depopulation of the states indicates an overestimation of the ionization effect by the model for elevated laser intensities. Comparison of the results obtained by the open system with those of the closed system presented in [33] indicates that taking into account the ionization slightly improves the fit with the experimental data presented in that work for low pump intensities. However, for the elevated laser intensities and atomic densities in Fig. 4b, our simplified ionization model leads to more than 50% of ionized atoms that no longer participate in the calculations and thus to reduced emissions.

In order to correctly evaluate the ionization effect for our experimental data, we note that both theoretical calculations and experimental results show a transition from a nonlinear to a saturation region above a critical intensity (as was already observed in [33] for an unfocused laser beam geometry and lower atomic densities). Taking into account this critical intensity, it is easily verified that theoretical calculations fit the experimental results well if the intensity used in the model is reduced by a factor of ~5000.

4.2 Path-2

Figure 3b, c shows the normalized energy plots for the emissions near the $|2\rangle \leftrightarrow |3\rangle$ and $|3\rangle \leftrightarrow |1\rangle$ transitions for the same atomic density of $N_{\max} = 1.5 \times 10^{15}$ cm^{-3}.

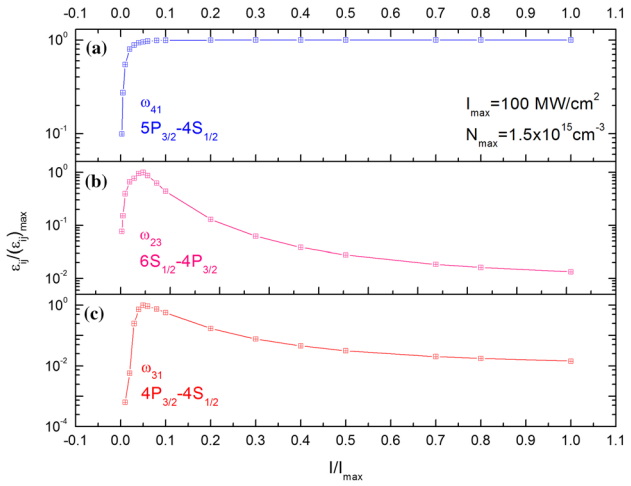

Fig. 3 Theoretical calculations of the normalized energy emitted at: **a** $|4\rangle \leftrightarrow |1\rangle$, **b** $|2\rangle \leftrightarrow |3\rangle$ and **c** $|3\rangle \leftrightarrow |1\rangle$ transitions, as a function of the normalized laser intensity used in the open four-level atomic system. The atomic density was $N_{\max} = 1.5 \times 10^{15}$ cm^{-3}, and the laser was tuned on the two-photon resonance $\Delta_{12} = 0$. Only axial propagation was taken into account in the calculations

The ionization rates used were $\Gamma_{\text{ion}} = 9$ cm^2/J and $\Gamma'_{\text{ion}} = 4.5$ cm^2/J. A peak is evident for both emissions at a pump intensity of $I_{\max} = 8$ MW/cm^2. For higher pump intensities the response is quite different when compared to that of path-1, the energy emitted in path-2 decays with increasing pumping intensity, while in path-1 remains saturated. This is strong evidence that two-photon resonant ionization negatively affects any process that needs high population transfer (ASE), which is the case in path-2 as was presented in [32, 33], but it does not affect much coherent processes (PFWM), which are dominant in path-1. However, our model may overestimate the ionization effect for high intensities although this was not possible to be experimentally verified for the laser pump intensities experimentally available.

Figure 5a, c shows the calculations for the normalized energy of the emissions in path-2 with increasing pump intensity for a collision rate of $\gamma_{\text{col}} = 0.0085$ cm^{-1} which corresponds to 10 mbar of buffer gas pressure. In order to overcome the overestimation of the ionization effect by our model for high intensities, we limit our focus on intensities that fit well with the experimental results. The experimental results are shown in Fig. 5b, d. The maximum peak intensity used in Fig. 5 for the model calculations was 20 MW/cm^2, while the maximum experimental intensity was 94 GW/cm^2.

A threshold for the generation of the emission at ω_{31} is observed for an experimental pumping intensity of approximately 10 GW/cm^2. Similar characteristics are evident for the theoretical calculations in Fig. 5d, with a threshold pump intensity of 2 MW/cm^2. Both in experimental and theoretical plots, emission at ω_{23} starts at much lower pump intensities and it appears that at the threshold intensity the emission at ω_{23} starts to saturate. This is an

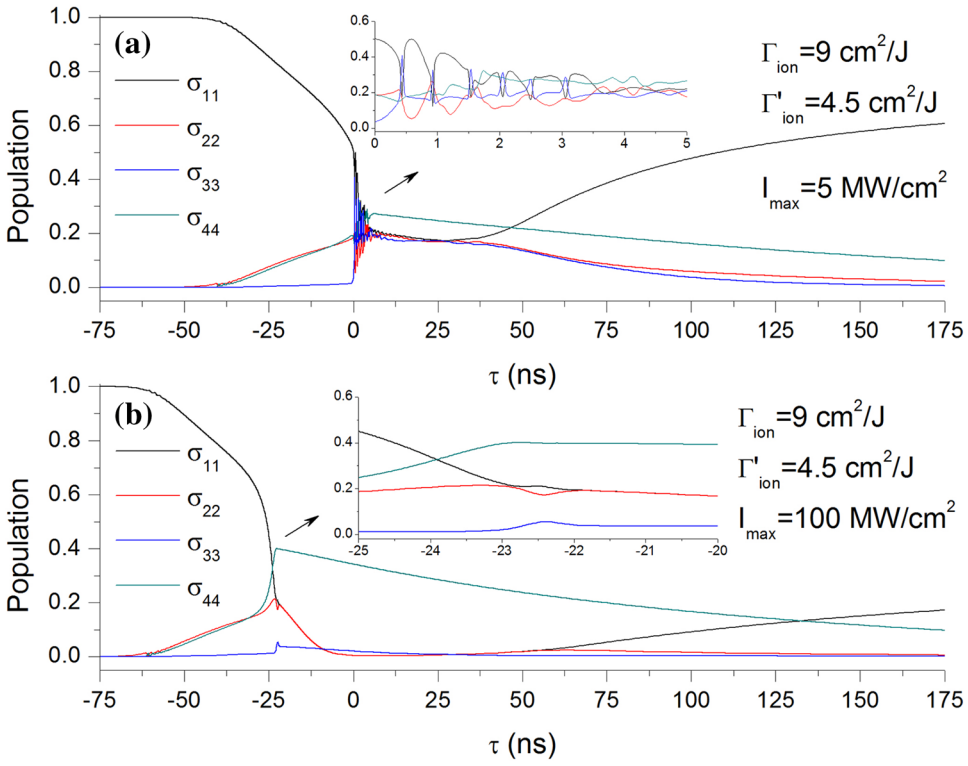

Fig. 4 Theoretical calculations of the population distribution in the open four-level atomic system. The laser peak intensity was: **a** $I_{\max} = 5$ MW/cm^2 and **b** $I_{\max} = 100$ MW/cm^2, respectively. The atomic density was $N_{\max} = 1.5 \times 10^{15}$ cm^{-3} and the potassium–buffer gas collision rate was $\gamma_{\text{col}} = 0.017$ s^{-1}. The ionization rates for the $|2\rangle$ and $|4\rangle$ states were $\Gamma_{\text{ion}} = 9$ cm^2/J and $\Gamma'_{\text{ion}} = 4.5$ cm^2/J, respectively

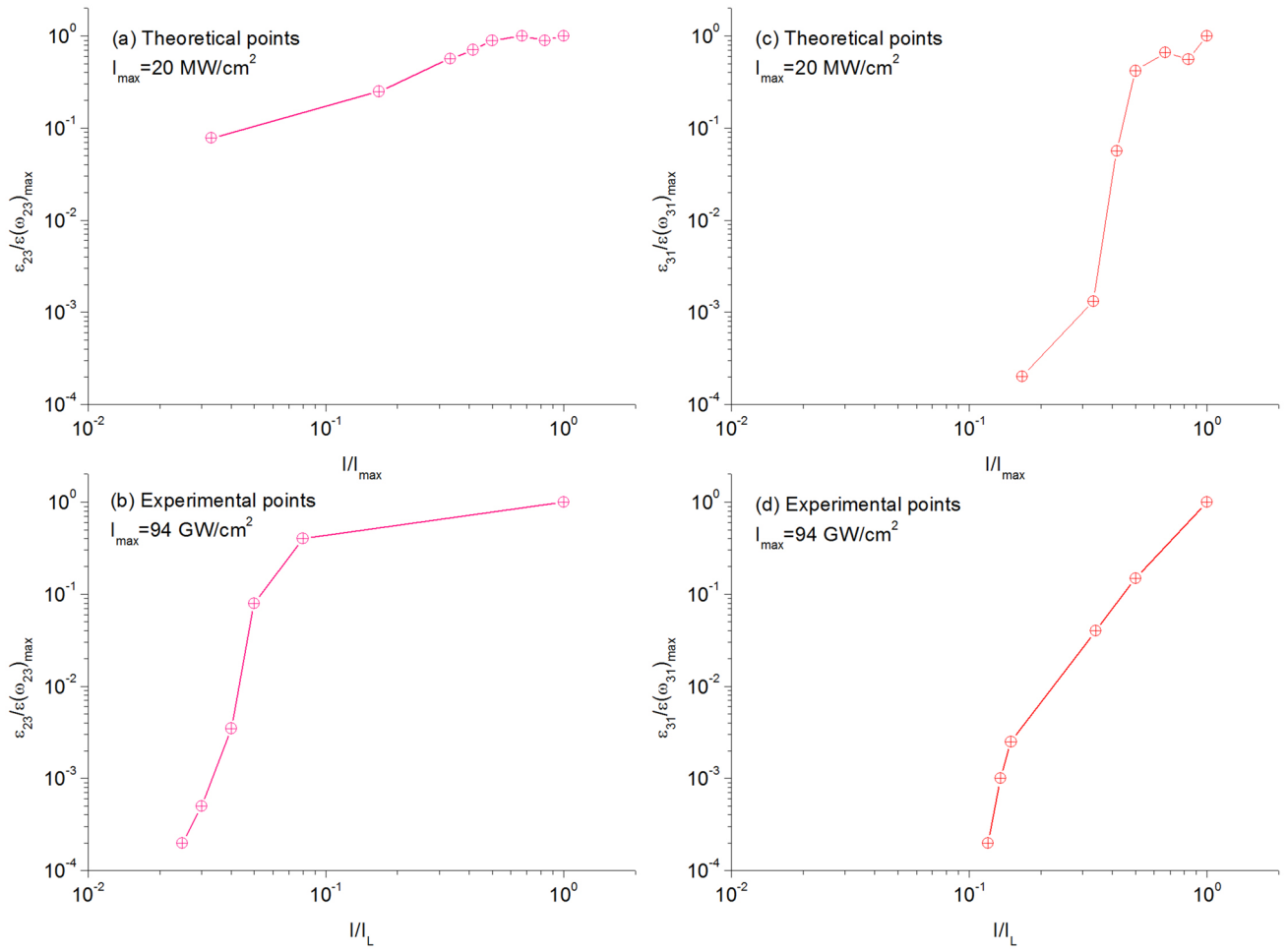

Fig. 5 Normalized energies of the emissions at ω_{23} and ω_{31} as a function of the normalized peak laser intensity. **a, c** show the theoretical calculations, while **b, d** present the experimental data. The atomic density was $N_{\max} = 1.5 \times 10^{15}$ cm^{-3} and the potassium–buffer gas pressure was 10 mbar ($\gamma_{\text{col}} = 0.0085$ s^{-1})

indication that emissions in path-2 are not due to PFWM, since in this case the intensity should be similar (since photons energies at ω_{23} and ω_{31} are approximately the same) and the saturation pump intensity threshold should be similar for both emissions. However, FWM processes that are not parametric could be dominant, as is explained below. The main mechanism of emission at ω_{23} and $\omega_{31}$was experimentally shown to be ASE in previous works of our group (in the case of ns excitation but for lower atomic densities and unfocused laser beam) since radiation was emitted also in the backward direction [32, 33]. In our case of using a focused laser beam and a subsequent shorter propagation length, it was not possible to experimentally detect the backward propagating ω_{31} emission. In addition, for pump intensities near and slightly above the threshold intensity, there is no or insignificant population inversion between ground state and state $|4P_{3/2}\rangle$, as is shown in Fig. 4a. In previous works [32, 33] the emission at ω_{31} was also proved to be produced without population inversion (their calculations were based on a closed atomic system).

For high intensities in the ns case or under fs excitation, a two-step FWM should play an important role [3, 4], where emission at ω_{23} is generated first and in a second step the mixing with two laser photons produce emission at ω_{31}. In this case ASE mechanism can be suppressed when the FWM process is strong enough [27]. In addition, the propagation length in our experiments (focused laser beam) is much shorter than in previous works, where the pump laser beam was unfocused. Consequently, the phase-matching is easier leading to more efficient FWM generation. It is expected in this case that the internally generated field at ω_{23} with a wavelength of 693.88 nm, which couples $|6S_{1/2}\rangle$ to $|4P_{3/2}\rangle$, enhances the third-order nonlinear susceptibility of wave mixing processes in path-2. When this field is strong enough, with a Rabi frequency larger than the widths of the states,

then a transparency window is induced that reduces absorption from ground state to $|4P_{3/2}\rangle$. This permits the efficient generation of the ω_{31} radiation near 766.49 nm. Experimental results in a similar atomic system [3, 4] showed that in order to induce this kind of transparency, the Rabi frequency of the coupling transition should be larger than the width of the $|6S_{1/2}\rangle$. In our experiment, the broadening of the state $|2\rangle$ was dominated by elastic collisions (0.017 cm^{-1}) and the calculated Rabi frequency for the ω_{23} radiation in the ns excitation case was 0.61 cm^{-1} when $I_L = 10$ GW/cm^2 (threshold intensity), a factor of 6 larger than the width of the state.

It was shown in [13–15] that FWM in atomic hydrogen can be enhanced and the absorption can be reduced, when a strong coupling laser is used besides the excitation laser. Resonant FWM was theoretically analyzed in [16] under conditions of EIT. The difference between those studies and ours is that in our case the coupling field, which corresponds to the $|2\rangle \leftrightarrow |3\rangle$ transition, is internally generated, it evolves nonlinearly and then it saturates when the pump intensity reaches a threshold value. Additionally, cascade generation of ASE or amplification without inversion (AWI) in a three-level system is also possible, under certain conditions [17, 20, 27, 33]. In the latter process, the generation of a strong radiation at ω_{23}can lead to a transparency window in the $|3\rangle \leftrightarrow |1\rangle$ transition and the efficient generation of ASE radiation at ω_{31} without population inversion. AWI could explain the lack of population inversion in the $|3\rangle \leftrightarrow |1\rangle$ transition for excitation intensities near the threshold intensity, as is shown in Fig. 4a. Both experimental results and theoretical calculations in Fig. 5 show that the saturation of the $|2\rangle \leftrightarrow |3\rangle$ emission is accompanied by the efficient generation of the $|3\rangle \leftrightarrow |1\rangle$ emission, which indicates that a transparency window is induced at the $|3\rangle \leftrightarrow |1\rangle$ transition, though it is difficult to conclude about the exact generation mechanism for the ω_{31} radiation. Above a certain excitation intensity value (that lead to the emissions peaks in Fig. 3 b, c), emissions in both transitions are affected by the two-photon resonant, three-photon ionization mechanism and control of the coupling field on the lower emission is reduced.

Despite the approximations made in the theoretical model, the curves in Fig. 5c, d appear to have the same characteristics in comparison to the experimental ones (Fig. 5a, b). The proposed control method can be generalized in similar systems in which a strong ns or fs pump excites and saturates partially coherent cascade emissions such as ASE, which can activate and control the emission at a lower transition. For example, similar results are experimentally recorded for the fs excitation case as it is shown in Fig. 2, where a pump energy threshold exists for efficient emission at the $|3\rangle \leftrightarrow |1\rangle$ transition. Note that conical FWM processes are dominant in the fs case, as is evident from the spatial profiles recorded in Fig. 2b–d, which are broad and indicative of phase-matching mechanisms. This means that our simplified model, which takes into account only axial propagation, can partially explain the spatial features of the emissions and thus a more elaborate model is necessary.

4.3 The atomic density effect in path-2

The effect of the potassium atomic density on the path-2 emissions is shown in Fig. 6. The theoretically calculated normalized energy of the emissions versus the normalized atomic density is shown in Fig. 6a, c and the experimental results in Fig. 6b, d. The increase of the precursor radiation at ω_{23} is connected with an almost similar increase of the radiation at ω_{31}, for potassium–buffer gas collision rate of $\gamma_{col} = 0.041$ cm^{-1}. There is an observable threshold in the detection of both radiations. Increase of the atomic density (up to $N'_{max} = 3.5 \times 10^{15}$ cm^{-3}) leads to linear response for both emissions, while initially the response is nonlinear. This effect is probably due to the increased absorption, which is exponentially depended on the density and the inefficient phase-matching for the FWM processes that also depends on the atomic density. It is noted that a similar initially nonlinear response was observed in the past [30] for the radiation of $|7S\rangle \leftrightarrow |6P\rangle$ transitions in mercury.

5 Conclusions

It is shown that the strong internally generated radiation at ω_{23} (upper transition $|6S_{1/2}\rangle \leftrightarrow |4P_{3/2}\rangle$), can act as an internal coupling field for the initiation of the lower emission at ω_{31} (lower transition $|4P_{3/2}\rangle \leftrightarrow |4S_{1/2}\rangle$) in the potassium atomic system. The role of ω_{23} as an internal coupling is examined, varying the critical system's parameters such as the pump peak intensity and the atomic density. In both cases ω_{23} acted as a threshold field for the production of a less strong field at ω_{31}.

Theoretical calculations for an open atomic system, which takes into account ionization processes, are backed by experimental results and show that coherent processes are not strongly affected by the transition to continuum for low intensities. Finally, an emission control method is proposed, where the external pump leads to an internally generated coupling field, which under a cascade configuration can activate and control the emission of a lower transition.

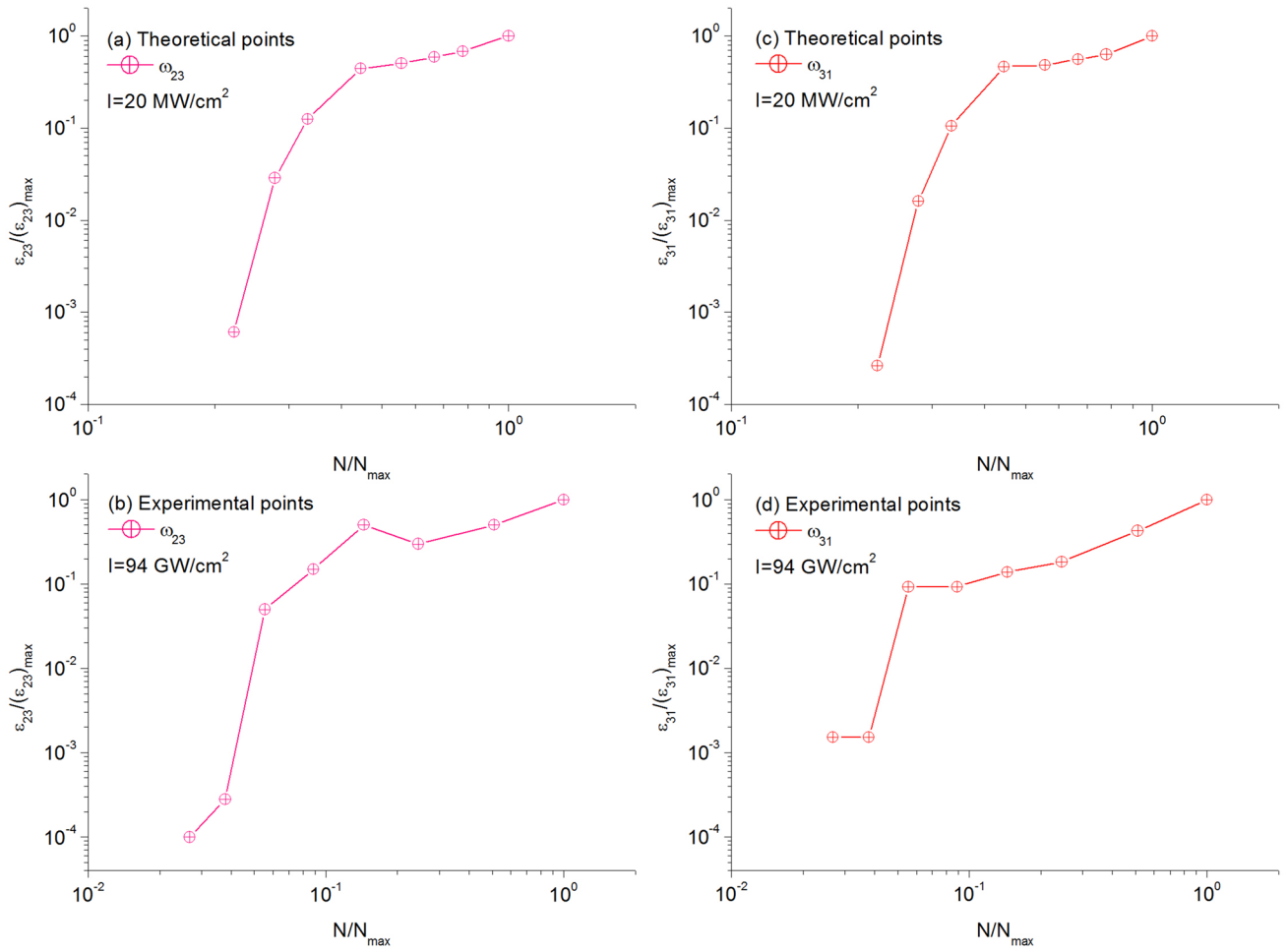

Fig. 6 Normalized energies of the emissions at ω_{23} and ω_{31} as a function of the potassium atomic density. **a, c** show the theoretical calculations, while **b, d** the experimental ones. The maximum atomic density was $N'_{\max} = 3.5 \times 10^{15}$ cm^{-3}. The potassium–buffer gas collision rate was 65 mbar ($\gamma_{\text{col}} = 0.041$ s^{-1})

Acknowledgements This project has received funding from the European Union's Horizon 2020 research and innovation programme under Grant agreement no. 654148 Laserlab-Europe.

References

1. E. Koudoumas, T. Efthimiopoulos, Appl. Phys. B **55**, 355 (1992)
2. E. Koudoumas, T. Efthimiopoulos, IEEE, J. Quant. Electron. **31**, 365 (1995)
3. M. Katharakis, N. Merlemis, A. Serafetinides, T. Efthimiopoulos, J. Phys. B **35**, 4969 (2002)
4. N. Merlemis, M. Katharakis, E. Koudoumas, T. Efthimiopoulos, J. Phys. B **36**, 1943 (2003)
5. N. Merlemis, M. Katharakis, E. Koudoumas, T. Efthimiopoulos, SPIE **5131**, 83 (2003)
6. M. Katharakis, N. Merlemis, A. Serafetinides, T. Efthimiopoulos, SPIE, **5131**, 73 (2003)
7. V. Vaičaitis, A. Piskarskas, Opt. Comm. **117**, 137 (1995)
8. V. Vaičaitis, E. Gaizauskas, Phys. Rev. A **75**, 033808 (2007)
9. V. Vaičaitis, S. Paulikas, Appl. Phys. B **89**, 267 (2007)
10. S.E. Harris, J.E. Field, A. Imamoglu, Phys. Rev. Lett. **64**, 1107 (1990)
11. K.J. Boiler, A. Imamoglu, S.E. Harris, Phys. Rev. Lett. **66**, 2593 (1991)
12. J.E. Field, K.H. Hahn, S.E. Harris, Phys. Rev. Lett. **67**, 3062 (1991)
13. K. Hakuta, L. Marmet, B.P. Stoicheff, Phys. Rev. A **45**, 5152 (1992)
14. G.Z. Zhang, K. Hakuta, B.P. Stoicheff, Phys. Rev. Lett. **71**, 3099 (1993)
15. R.I. Thomson, B.P. Stoicheff, G.Z. Zhang, K. Hakuta, J. Quant. Opt. **6**, 349 (1994)
16. V.G. Arkhipkin, Opt. Spectrosc. **79**, 248 (1995)
17. Y. Zhu, Phys. Rev. A **47**, 495 (1993)
18. Y. Zhu, Opt. Comm. **105**, 253 (1994)
19. Y. Zhu, Opt. Comm. **107**, 499 (1994)
20. S.-Q. Gong, H.-G. Teng, Z.-Z. Xu, Phys. Rev. A **51**, 3382 (1995)
21. P.L. Zhang, Y.,-C. Wang, A.L. Schwalow, J. Opt. Soc. Am. B **1**, 9 (1984)
22. B.K. Clark, M. Masters, J. Huennekens, Appl. Phys. B **47**, 159 (1988)
23. Z.J. Jabbour, M.S. Malcuit, J. Huennekens, Appl. Phys. B **52**, 281 (1991)

24. T. Efthimiopoulos, M.E. Movsessian, M. Katharakis, N. Merlemis, J. Appl. Phys. **80**, 2 (1996)
25. S.M. Hamadi, J.A.D. Stockdale, R.N. Compto, M.S. Pindzola, Phys. Rev. A, 34, 1938, (1986)
26. M.A. Moore, W.R. Garrett, M.G. Payne, Opt. Comm. **68**, 310 (1988)
27. M.S. Malcuit, D.J. Gauthier, R.W. Boyd, Phys. Rev. Lett. **55**, 1086 (1985)
28. W.R. Garrett, Phys. Rev. Lett. **70**, 4059 (1993)
29. M.E. Movsessian, A.V. Popoyan, S.V. Shmavonyan, Int. J. of Nonlinear Opt. Phys. **1**, 775 (1992)
30. N. Omenetto, O.I. Matveev, W. Resto, R. Badini, B.W. Smith, T.D. Winefordner, Appl. Phys. B **58**, 303 (1994)
31. L. Deng, M.G. Payne, W.R. Garrett, Phys. Rep. **429**, 123 (2006)
32. N. Merlemis, A. Lyras, M. Katharakis, T. Efthimiopoulos, J. Phys. B At. Mol. Opt. Phys. **39**, 1913 (2006)
33. A. Armyras, D. Pentaris, T. Efthimiopoulos, N. Merlemis, A. Lyras, J. Phys. B At. Mol. Opt. Phys. **44**, 165401 (2011)
34. D. Pentaris, T. Efthimiopoulos, N. Merlemis, V. Vaičaitis, A. Lyras, Appl. Phys. B **107**, 71 (2012)
35. D. Pentaris, T. Efthimiopoulos, N. Merlemis, A. Lyras, J. Mod. Opt. **59**, 179 (2012)
36. S.N. Dixit, P. Lambropoulos, Phys. Rev. A **24**, 318 (1981)
37. S.N. Dixit, P. Lambropoulos, Phys. Rev. A. **27**, 861 (1983)
38. E. Gaižauskas, D. Pentaris, T. Efthimiopoulos, V. Vaičaitis, Opt. Lett. **38** 124 (2013)
39. D. Pentaris, G. Papademetriou, T. Efthimiopoulos, N. Merlemis, A. Lyras, J. Mod. Opt. **60**, 1855 (2013)
40. G. Papademetriou, D. Pentaris, T. Efthimiopoulos, A. Lyras, J. Phys. B At. Mol. Opt. Phys. **50**, 125401 (2017)
41. D. Pentaris, D. Damianos, G. Papademetriou, A. Lyras, K. Steponkevičius, V. Vaičaitis, T. Efthimiopoulos, J. Mod. Opt. **63**, 1301 (2016)